Title:
Miro recruits VPS13D to mitochondria

Authors: Andrés Guillén-Samander[1#], Marianna Leonzino[1#], Pietro De Camilli[1,2*]
[1]Departments of Neuroscience and of Cell Biology, Howard Hughes Medical Institute, Program in Cellular Neuroscience, Neurodegeneration and Repair, [2]Kavli Institute for Neuroscience, Yale University School of Medicine, New Haven, Connecticut 06510, USA;
[#] Equal contributions
[*]Corresponding author

Acknowledgements:
We thank M. Hanna, H. Falahati and J.H. Park for discussion and N. Tang, F. Wilson and A. Dao for outstanding technical assistance. This work was supported in part by NIH grant NS36251, the HHMI, the Kavli Foundation and the Parkinson's Foundation (PF-RCE-1946) to P.D.C. A.G.S. was supported by a Jung-Stiftung Scholarship.

Summary:

Protein-mediated ER-mitochondria lipid transfer is critical for eukaryotic cells. However, the underlying machinery is not well conserved. Guillén-Samander et al, show that Gem1/Miro is an evolutionary conserved link between the yeast ERMES complex and the mammalian lipid transfer protein VPS13D.

Abstract:

Mitochondria, which are excluded from the secretory pathway, depend on lipid transport proteins for their lipid supply from the ER, where most lipids are synthesized. In yeast, the outer membrane GTPase Gem1 is an accessory factor of ERMES, an ER-mitochondria tethering complex that contains lipid transport domains and plays a function, partially redundant with VPS13, in lipid transfer between the two organelles. In metazoa, where VPS13, but not ERMES, is present, the Gem1 orthologue Miro has been linked to mitochondrial motility but not to lipid transport. Here we show that Miro recruits to mitochondria the lipid transport protein VPS13D which, like Miro, is an essential protein in mammals, and whose localization had remained elusive. We also show that VPS13D can tether mitochondria to the ER in a Miro- and VAP-dependent way. These findings reveal a so far missing link between function(s) of Gem1/Miro in yeast and higher eukaryotes, where Miro is a Parkin substrate, with potential implications for Parkinson's disease pathogenesis.

Introduction:

Homeostasis of membranous subcellular organelles relies on appropriate synthesis, metabolism and distribution of bilayer lipids. Most such lipids are synthesized in the ER and their delivery to other destinations relies both on vesicular traffic and on protein-mediated lipid transfer. Much of the latter route of delivery occurs at membrane contact sites where many lipid transport proteins also function as tethers between the two membranes. For mitochondria, which are excluded from the membrane traffic flow of the secretory pathway, protein-mediated lipid transfer represents the only mechanism for their supply of lipids from the ER. In yeast, ERMES, a heterotetrametric protein complex that contains lipid transport modules and tethers the ER to the outer mitochondrial membrane (OMM) was shown to account for some of this transport(Kornmann et al., 2009). Another yeast protein, Vps13, which also localizes at membrane contact sites, albeit not ER-mitochondria contacts in this organism, was shown to have partially overlapping function with ERMES, possibly by participating in an alternative route for the delivery of lipids from the ER to mitochondria via the vacuole (Park et al., 2016; John Peter et al., 2017). While the ERMES complex is not conserved in metazoans, the single yeast Vps13 has 4 different homologues in mammals (including in humans), suggesting a more critical function of this protein family in mammalian cells(Velayos-Baeza et al., 2004). Additionally, an accessory subunit of ERMES, the GTPase Gem1, is also conserved in higher eukaryotes (Frederick et al., 2004; Kornmann et al., 2011).The two mammalian Gem1 orthologues, however, Miro1 and Miro2, have been associated primarily with mitochondrial motility and not with lipid transport (Fransson et al., 2003; Glater et al., 2006; Saotome et al., 2008; Macaskill et al., 2009; Wang and Schwarz, 2009; Nguyen et al., 2014), although a localization of Miro at ER-mitochondria contacts sites has also been reported (Kornmann et al., 2009; Modi et al., 2019).

Recent findings have shown that VPS13 is indeed a lipid transport protein and shed light on the molecular properties of VPS13 family proteins and on some of their sites of action in animal cells(Kumar et al., 2018; Li et al., 2020). The N-terminal portion of VPS13 folds as an elongated tube with a hydrophobic groove that runs along its entire length, thus suggesting that VPS13 acts as a bridge allowing lipid flow from one bilayer to another at sites of bilayer apposition (Li et al., 2020; Lees and Reinisch, 2020; Ugur et al., 2020). Such structure may account for net transfer of lipids and thus for a role of VPS13 and of its distant relative ATG2 (Kumar et al., 2018), an autophagy protein with a very similar fold(Valverde et al., 2019; Osawa et al., 2019; Maeda et al., 2019), in membrane expansion. Studies of mammalian VPS13A and VPS13C have demonstrated that they not only are localized at membrane contact sites, but also tether adjacent membranes(Kumar et al., 2018). Moreover, studies of the mammalian VPS13 protein family have shown isoform-specific localizations (Seifert et al., 2011; Kumar et al., 2018; Yeshaw et al., 2019). VPS13A populates ER-mitochondria contacts, where it may have taken over some of the functions of ERMES, VPS13C is localized at ER-late endosomes/lysosome contacts(Kumar et al., 2018) and VPS13B resides predominantly in the Golgi complex region (Seifert et al., 2011). The localization and potential tethering properties of VPS13D remain unclear. Distinct functions of the four mammalian VPS13 proteins are further demonstrated by the different neurological diseases associated with their loss-of-function mutations, namely chorea acanthocytosis (VPS13A)(Rampoldi et al., 2001; Ueno et al., 2001), Cohen syndrome (VPS13B)(Kolehmainen et al., 2003), Parkinson's disease (VPS13C)(Lesage et al., 2016; Schormair et al., 2018) and ataxia (VPS13D)(Gauthier et al., 2018; Seong et al., 2018).

VPS13D is the only mammalian VPS13 protein proven to be essential for life, as its absence in mice leads to embryonic lethality, and in flies leads to death at the larval stage(Seong et al., 2018; Anding et al., 2018). While complete absence of each of the other three VPS13 proteins is compatible with life in humans, albeit with developmental (VPS13B) or neurodegenerative (VPS13A and VPS13C) defects, in patients with compound heterozygous VPS13D mutations leading to severe ataxias at least one of the alleles carries a missense mutation, thus probably encoding an at least partially functioning protein(Dziurdzik et al., 2020; Ugur et al., 2020). Given its physiological importance, investigation of this protein will likely reveal some fundamental aspect of the biology of the VPS13 protein family. Studies in both human cells and flies have suggested a role for VPS13D in mitochondrial function. Enlarged spherical mitochondria have been reported in VPS13D-KD fly midgut cells and neurons, in VPS13D-KO HeLa cells and in patient-derived fibroblasts(Seong et al., 2018; Anding et al., 2018; Insolera et al., 2020). However, so far, VPS13D has not been visualized in association with mitochondria, and was instead reported, based on immunofluorescence of its orthologue in Drosophila, to be localized on lysosomes(Anding et al., 2018).

Here we show that VPS13D can localize to mitochondria, where it is recruited by the outer mitochondrial GTPases Miro1 and Miro2. These findings suggest that, like its yeast orthologue Gem1, Miro participates in the control of lipid transport

between the ER and mitochondria, thus revealing an evolutionary link between the functions of Miro and Gem1 that had remained elusive until now. We also show that VPS13D can tether mitochondria to the ER via a mechanism that depends on Miro and on the ER protein VAP. Collectively, our results provide new insight into the crosstalk between the ER and mitochondria at their contact sites and into the mitochondrial phenotypes caused by the lack of VPS13D.

Results and Discussion:

VPS13D, with 4388 residues in humans, is the largest protein of the human VPS13 family. Its predicted domain architecture is overall very similar to that of other VPS13 proteins (Velayos-Baeza et al., 2004; Kumar et al., 2018). It comprises a long N-terminal lipid transfer domain that starts with the conserved chorein domain and is predicted to be slightly longer than in other VPS13 isoforms, a β-propeller region (so called VAB (Dziurdzik et al., 2020) or WD40-like region(Kumar et al., 2018)), a DH-like domain and a C-terminal PH domain. Differently from other human VPS13 proteins, VPS13D also contains a ubiquitin-binding domain (UBA) (Fig. 1A, left). To investigate VPS13D localization in cells, overcoming the limited expression expected upon transfection of such a large protein, a synthetic codon optimized cDNA sequence encoding VPS13D was generated, which also included a fluorescent tag (Halo or EGFP) after residue 1576 (hereafter referred to as VPS13D^tag). This position, which is localized in a predicted disordered loop, corresponds to the position where tag insertion did not to affect function in other VPS13 proteins (Park et al., 2016; Kumar et al., 2018) (Fig. 1A). Expression of VPS13D^EGFP in COS7 cells resulted in a diffuse cytosolic fluorescence with some variable accumulation in the Golgi complex region and a weak enrichment, also variable in intensity from cell to cell, but detectable in about half of the cells, around mitochondria (Fig. 1B). In cells where such localization was detectable, VPS13D was not restricted to a small subset of mitochondria, speaking against a selective binding of VPS13D via its UBA domain to ubiquitinated mitochondria targeted to degradation.

Among the outer mitochondrial membrane (OMM) proteins that could function as regulated binding partners for VPS13D at the mitochondrial surface, we considered Miro1 and Miro2 (henceforth referred to as Miro) as potential candidates. Miro, which contains two GTPase domains and two EF-hand Ca^{2+}-binding domains exposed to the cytosol (Fig. 1A, right), has been primarily implicated in the regulation of mitochondrial transport in mammalian cells (Fransson et al., 2003; Glater et al., 2006; Saotome et al., 2008; Macaskill et al., 2009; Wang and Schwarz, 2009; Nguyen et al., 2014). The Miro orthologue in yeast, Gem1, is an accessory subunit of the ERMES complex, whose function in lipid transport between ER and mitochondria is partially redundant with that of yeast Vps13 (Lang et al., 2015; Park et al., 2016). Thus, a potential connection of Miro to a mammalian VPS13 family member seemed plausible. When either EGFP-Miro1 or EGFP-Miro2 were co-expressed with VPS13D^Halo in COS7 cells, a major impact on the localization of VPS13D^Halo was observed. This protein was now strikingly concentrated on mitochondria in more than 85% of the cells, where it colocalized with Miro along the entire mitochondrial surface (Fig. 1C and D and Fig. S1A) with minimal residual fluorescence elsewhere in the cell. Colocalization of co-transfected VPS13D^Halo and EGFP-Miro1 was also observed in mouse hippocampal neurons, where VPS13D was recruited to mitochondria both in the cell soma and in the neurites (Fig. 1E). A splice variant of Miro1 (transcript variant 4, referred to as Miro1v4) was previously shown to localize predominantly in the outer peroxisomal membrane and only weakly on the OMM(Okumoto et al., 2018). Upon co-expression of this Miro isoform, the majority of VPS13D^Halo was recruited on peroxisomes where Miro1v4 was enriched, and for both proteins only faint signal was observed on mitochondria (Fig.1F). These results strongly argue for a Miro-mediated recruitment of VPS13D to mitochondria and to peroxisomes.

To further validate the importance of Miro in VPS13D recruitment, the iLID optical dimerization system(Guntas et al., 2015) was used to induce acutely, upon blue light illumination, the association of the cytosolic portion of Miro to the mitochondrial surface. We co-transfected VPS13D^Halo with a mitochondrial anchored bait (iLID fused to the mitochondrial targeting region of ActA), and the cytosolic portion of Miro1 fused to the cognate pray for iLID (the SspB peptide). Blue light illumination induced immediate massive recruitment of the Miro1 construct to mitochondria which was followed by a corresponding massive recruitment of VPS13D Fig. 1G). Conversely, upon light interruption, both proteins were shed from mitochondria (Fig. 1G and Movie S1). However, shedding of VPS13D followed only with some latency the shedding of Miro (Fig. 1H), revealing that once VPS13D is recruited to mitochondria its persistence at their surface is not strictly dependent on the presence of Miro. Whether this finding reflects only an indirect role of Miro in VPS13 recruitment, or the occurrence of stabilizing VPS13D interactions at the mitochondrial membrane after a direct recruitment by Miro remains to be determined. A direct interaction between Miro and VPS13D could not be convincingly demonstrated by co-precipitation.

Miro1 constructs with inactivating mutations (Fransson et al., 2003; Frederick et al., 2004) in the GTP binding site of the N-GTPase domain (T18N) or in the Ca^{2+}-binding sites of both EF hands (E208K/E328K) (Fig. 2A) no longer promoted

recruitment of VPS13D to mitochondria (Fig. 2B). In contrast, a mutation in the C-GTPase (S432N) did not affect such recruitment of VPS13D (Fig. 2B). Similar results were obtained for the binding of Miro1 to other interactors and for the binding of Gem1 to ERMES in yeast(Kornmann et al., 2011; Kanfer et al., 2015; Oeding et al., 2018). Whether some of the disrupting effects of these mutation is due to misfolding remains to be determined. In view of the impact produced by mutations in the EF hands, we analyzed whether elevations of cytosolic Ca^{2+} would affect binding of VPS13D to mitochondria in the presence of Miro. However, increases in cytosolic Ca^{2+} induced by inhibition of the SERCA ER Ca^{2+} pump by thapsigargin treatment did not impair VPS13D recruitment to mitochondria (Fig. S1B).

To determine the region of VPS13D required for Miro-dependent recruitment we co-expressed Miro with several VPS13D fragments. Removal of the C-terminal region of VPS13D including both the VAB/WD40-like domain and DH-PH domains, abolished its Miro-dependent recruitment to mitochondria (Fig. 2C). In contrast, VPS13D constructs lacking the DH-PH domain were still recruited by Miro, whereas constructs containing the DH-PH domain but not the VAB/WD40-like domain were not (Fig. 2C), suggesting that the VAB/WD40-like domain was necessary for this recruitment. However, Miro also did not trigger the recruitment to mitochondria of constructs comprising only the VAB/WD40-like domain (Fig. S2A), raising the possibility that another portion of full length VPS13D may be involved in this recruitment. It is also possible, that the constructs that we have generated may not fold correctly, as all of them produced intracellular aggregates in a subset of cells (Fig. S2B). VPS13A, a paralogue of VPS13D, also binds mitochondria, and it does so via its C-terminal DH-PH domain whose interactor(s) at the mitochondrial surface remain(s) unknown(Kumar et al., 2018). However, co-transfection of VPS13A with Miro1 did not result in an increased recruitment of VPS13A to mitochondria (Fig. S1C). This indicates an at least partially different way of mitochondrial binding of VPS13A and VPS13D.

Studies of yeast Vps13 and of mammalian VPS13A and VPS13C have shown that a shared property of these proteins is to bridge organelles to provide a conduit for the flow of lipids between adjacent bilayers. Both VPS13A and VPS13C tether other organelles to the ER via an interaction of their FFAT motifs with the MSP domain of the ER proteins VAPA and VAPB (Kumar et al., 2018). Thus, we explored whether VPS13D does the same. No obvious fluorescence signal on the ER was observed when VPS13D^EGFP was expressed alone (Fig. 1B), but co-transfection with Halo-VAPB resulted in a partial colocalization of VPS13D^EGFP with VAPB on the ER (Fig. 3A) Most likely, endogenous VAP expression levels are not sufficient to bind a detectable amount of VPS13D and/or the diffuse cytosolic fluorescence of VPS13D^EGFP obscures such localization. Overexpression of VAPB, but not of a VAPB mutant defective in FFAT motif binding(Dong et al., 2016), also induced the recruitment to the ER of the VPS13D N-terminal region alone, indicating that the ER binding site, as in the case of VPS13A and VPS13C, lies somewhere in this region (Fig. 3B and Fig. S3C). Three FFAT motifs are predicted with low score(Murphy and Levine, 2016; Slee and Levine, 2019) in this portion of VPS13D, but the combined mutation of all three sites did not abolish VAP-dependent recruitment to the ER, raising the possibility of an alternative, possibly indirect, way of binding (Fig. S3**).** Note that VPS13A was efficiently recruited to the ER in a VAP-dependent way without VAP overexpression(Kumar et al., 2018), suggesting differences in either the affinity for VAP or the occurrence of different regulatory mechanisms.

Importantly, when BFP-VAPB was co-expressed with VPS13D^Halo and EGFP-Miro1, VPS13D^Halo signal no longer decorated the entire mitochondrial surface homogeneously but had a discontinuous pattern. The hot spots of fluorescence precisely colocalized with sites of apposition between the mitochondria and the ER, consistent with a localization of VPS13D at contacts between the two organelles (Fig. 3C). This conclusion was supported by observing VPS13D dynamics during exposure of cells to strong hypotonic solutions. Under these conditions, dramatic shape changes and organelle vesiculation occur, but tethers between organelles persist(King et al., 2020). In cells expressing all three proteins, VPS13D^Halo fluorescence coalesced at sites where mitochondria- and ER-derived vesicles remained in contact with each other, as it is expected for a tethering protein (Fig. 3D and Movie S2).

In conclusion, our findings demonstrate a Miro-dependent association of VPS13D with mitochondria and peroxisomes, as well as a VAP-dependent association of VPS13D with the ER. An association of VPS13D with mitochondria is also supported by recent proximity-labelling based studies listing this protein, as well as VPS13A (but not VPS13B or VPS13C), among the hits retrieved with OMM baits (Hung et al., 2017; Liu et al., 2018; Antonicka et al., 2020). Based on our results, VPS13D may have a partially overlapping role with VPS13A in lipid fluxes between the ER and mitochondria, but a more dominant function, as VPS13D is essential for life while VPS13A is not. Roles of VPS13D at other cellular sites, most likely mediated by other interactions, should also be considered, in view of its partial localization in the Golgi complex area.

Both VPS13D and Miro are essential for animal survival (López-Doménech et al., 2018; Seong et al., 2018). Moreover, in cellular models, loss-of-function of either Miro or VPS13D induce alterations in mitochondrial size, distribution and degradation(Nguyen et al., 2014; Anding et al., 2018; Seong et al., 2018; López-Doménech et al., 2018; Insolera et al., 2020), underscoring the strong physiological relevance of the results reported here. A role of Miro related to a lipid transport protein reveals an evolutionary link, missing so far, between the function of the Gem1/Miro family in fungi and mammals. Precisely how Miro recruits VPS13D, and the impact of the lipid transport function of VPS13D once recruited to mitochondria, remain questions for future studies. Among the many potential scenarios to be considered, one is that the altered mitochondrial morphology in cells lacking VPS13D may result from reduced membrane lipid availability for membrane expansion with an increase of volume to surface ratio. Swelling of mitochondria, in turn, may impair the action of the fission machinery. As Miro is a substrate for Parkin(Wang et al., 2011; Shlevkov et al., 2016), and is itself a target of Parkinson's Disease-associated mutations(Berenguer-Escuder et al., 2019), our results may also be relevant to pathogenetic mechanisms of Parkinson's diseases.

Figure legends

Figure 1. VPS13D recruitment by Miro GTPases. (A) Left: domain organization of human VPS13D. Some precise domain boundaries are not clear yet. Right: domain organization of human Miro1. (B) Confocal images of COS7 cells showing that VPS13D^EGFP decorates mitochondria, as shown by colocalization with mito-BFP (Inset 1), and is also enriched in the Golgi area, as shown by localization relative to with Sialyltransferase(ST)-Halo (Inset 2). (C) Transfection of Halo-Miro1, resulting in Miro1 overexpression, recruits co-expressed VPS13D^EGFP to the OMM. (D) Recruitment of VPS13D can also be achieved by co-expression with Miro2. (E) VPS13D^Halo and EGFP-Miro1 colocalize in the cell body and processes of mouse hippocampal neurons. (F) COS7 cells showing that VPS13D^Halo is recruited to peroxisomes upon co-expression with transcript variant 4 of Miro1, a splice variant that resides primarily in the peroxisomal membrane. The inset shows colocalization with the peroxisomal luminal marker mScarlet-SRL. (G) Optogenetic recruitment of the cytosolic domain of Miro1 to the OMM. Top panels: schematic representation of the experiment Venus-iLID-Mito in the OMM recruits mCh-Miro1(ΔTM)-SspB upon blue-light excitation. The recruitment of Miro1, in turn, triggers the recruitment of VPS13D. Mid and bottom panels: confocal images of a COS7 cell showing blue-light-dependent recruitment and shedding of mCh-Miro1(ΔTM)-SspB and correspondingly of VPS13D^Halo. The illumination was started at time 0sec, on a 5μm^2 area shown in the leftmost panel. See also Movie S1. Scale bars=10μm. (H) Both the recruitment and shedding of VPS13D^Halo are delayed relative to mCh-Miro1(ΔTM)-SSPB. Top panels: snapshots of an isolated mitochondrion at the peak of recruitment. Mid panels: example kymographs showing the increase and decrease in fluorescence along the stippled 3μm line traced across the mitochondrion of the top panels. The kymographs start 10s before stimulation. The fluorescence intensity along the length of these kymographs was measured and normalized (from 18 independently excited mitochondria in 14 different cells) and average values ±SEM are plotted in the bottom graph. The decay in intensity of VPS13D^Halo and mCh-Miro1(ΔTM)-SspB on mitochondria was fitted to an exponential equation: For VPS13D^Halo, time constant τ=86.51s, 95%CI [77.64, 97.56], for mCh-Miro1(ΔTM)-SspB time constant τ=54.11s, 95%CI [51.07, 57.54], adj. R-square of fits 0.97 and 0.98, respectively.

Figure 2. Recruitment of VPS13D by Miro GTPases requires their functional N-GTPase domain and EF-hands domains, and the β-propeller region of VPS13D. (A) Domain organization of human Miro1 with indication of the mutations used for the experiments of panel B. (B) Confocal images of COS7 cells showing that the recruitment of VPS13D^Halo by EGFP-Miro1 is impaired by mutations in the GTP binding site of its N-GTPase domain and in the Ca^{2+} binding sites of both its EF-hands, but not by a mutation in the GTP binding site of its C-GTPase domain. Scale bars=3μm. (C) Top: Cartoons showing VPS13D constructs used for the experiments shown below used. Bottom: Confocal images show that removal of a portion containing the β-propeller region abolishes recruitment of VPS13D^EGFP by Halo-Miro1. Scale bars=10μm

Figure 3. VPS13D can tether the ER to mitochondria in a VAP and Miro-dependent way. (A) Left: confocal image of a COS7 cell co-expressing Halo-VAPB and VPS13D^EGFP showing recruitment of VPS13D^EGFP to the ER. Scale bar=10μm. Right: high magnification view of Halo-VAPB and VPS13D^EGFP fluorescence of the field enclosed by a rectangle at left. (B) VAP-dependent binding of the N-terminal portion of VPS13D to the ER. Left: confocal images of a COS7 cell co-expressing the N-terminal portion of VPS13D fused to EGFP and Sec61β-RFP. Right: confocal images of a COS7 cell co-expressing the N-terminal portion of VPS13D fused to EGFP and mCherry-VAPB. (C) VPS13D^Halo is enriched at hot spots (white arrowheads) where the ER and mitochondria intersect when co-expressed with EGFP-Miro1 and BFP-VAPB

in a COS7 cell. (D) Vesiculated ER and mitochondria induced by hypotonic treatment of cells co-expressing VPS13D^Halo, GFP-Miro1 and BFP-VAPB remain tethered to each other, and VPS13D^Halo concentrates at these sites (white arrowheads). See also Movie S2. Scale bars=3μm.

Materials and Methods

Reagents and DNA plasmids

A plasmid containing codon-optimized cDNA encoding human VPS13D, also including an mScarlet fluorescent protein after aminoacid residue 1576 flanked by BamHI restriction enzyme sites, was generated by and purchased from Genscript. This plasmid was linearized with BamHI and used to clone VPS13D^EGFP and VPS13D^Halo by Infusion cloning (Takara). An N-terminal fragment of VPS13D, Nterm(VPS13D)^EGFP, and a deletion mutant of VPS13D lacking the B-propeller region (VAB/WD40-like domain), VPS13D(Δβ-prop)^EGFP, were generated by PCR amplification and ligated into pEGFP-C1 by Infusion cloning, using EcoRI and AgeI sites. A C-terminally truncated VPS13D, VPS13D(ΔDHPH)^EGFP, was generated using site-directed mutagenesis (QuikChange II XL; Agilent technologies) by adding an early stop codon replacing the codon encoding aminoacid residue 3802. Plasmids containing human Miro1(variant 1) and human Miro2 were a gift from P. Aspenström (Addgene #47888 and #47891). EGFP-Miro1, EGFP-Miro2 and mCherry-Miro1 were generated by PCR amplification of the coding sequence of Miro and ligated into pEGFP-C1(Addgene) or pmCherry-C1(Addgene), using EcoRI and XhoI sites. Halo-Miro1 was generated by PCR amplification of the coding sequence of Miro from EGFP-Miro1 and the coding sequence of the Halo protein from pHalo-C1 and ligated by Infusion cloning into a pcDNA3.1 backbone. For EGFP-Miro1v4 a double stranded DNA fragment encoding the aminoacid residues from exons 8 and 9 of Miro1 (i.e. the exons missing from Miro variant 1) was ordered from IDT and ligated into EGFP-Miro1 at residue 580 by Infusion cloning. For the optogenetic experiments, the cytosolic domain of Miro1 (Miro1(ΔTM)) and the iLID binding peptide (SspB, obtained from Addgene #60415, gift from B. Kuhlman) were fused into pmCherry-C1 using EcoRI and KpnI, by infusion cloning (mCh-Miro1(ΔTM)-SSPB). EGFP-Miro1 constructs containing mutations T18N, E208/E328K and S432N were generated using site-directed mutagenesis (QuikChange II XL; Agilent technologies) of EGFP-Miro1. To generate BFP-VAPB, the VAPB coding sequence was amplified by PCR from a mCherry-VAPB plasmid (our laboratory), the BFP coding sequence was amplified from mitoBFP (Addgene#49151) and were assembled by HiFi reaction (NEB). HALO-VAPB was obtained by PCR amplification of VAPB coding sequence from mCherry-VAPB and pHALO-C1 using EcoRI and KpnI sites. Sialyltransferase(ST)-Halo was generated by PCR amplification of the ST coding sequence from ST-mRFP (our laboratory) and ligated into pHALO-N1 using EcoRI and KpnI sites. Other plasmids used in this study were kind gifts: mito-BFP from G. Voeltz (Addgene #49151), Venus-iLID-Mito from B. Kuhlman (Addgene #60413), mScarlet-SRL from D. Gadella (Addgene #85063). Mutant VAPB (K87D, M89D) was previously generated in our lab(Dong et al., 2016). Halo tag ligands were a kind gift from L. Lavis (Janelia Farm, Ashburn, VA). For specific primers used refer to Supplementary Table 1.

Cell culture and transfection

COS7 cells (from ATCC) were cultured at 37ºC and 5% CO2 in DMEM containing 10%FBS, 1mM sodium pyruvate, 100U/ml penicillin, 100mg/mL streptomycin and 2mM L-glutamine (all from Gibco). For imaging experiments, cells were seeded on glass-bottomed dishes (MatTek) at a concentration of $75x10^3$ cells per dish and transiently transfected after 6h using FuGene HD (Promega).

Neuronal cultures

Experiments were performed in accordance with the Yale University Institutional Animal Care and Use Committee. Briefly, hippocampi were dissected from P0 mouse brains, neurons were dissociated by papain treatment and seeded in serum-based medium on poly-D-lysine coated, glass-bottomed dishes (MatTek), as previously described {Sun 2019}. After six hours, the serum-based medium was removed and replaced with neuronal growth media [Neurobasal A supplemented with B27 and Glutamax (all from Gibco)]. After 11 DIV, cells were transfected using Lipofectamine 2000 (Life Technologies).

Microscopy

Live cell imaging. Just before imaging, the growth medium was removed and replaced with Live Cell Imaging solution (Life technologies). All live cell imaging was carried out at 37ºC and 5%CO_2. Spinning-disk confocal microscopy was performed using an Andor Dragonfly system equipped with a PlanApo objective (63X, 1.4NA, Oil) and a Zyla sCMOS camera. For the hypotonic lysis experiments, Live Cell Imaging solution was replaced with distilled water and cells were imaged at a rate of 0.5Hz.

Optogenetic experiments. For whole cell activation experiments, an Andor Dragonfly system (see above) was used and recruitment to mitochondria was achieved with a single 200ms pulse of the 488nm laser. For localized activation to promote recruitment to a single mitochondrion, an Improvision UltraVIEW VoX system (Perkin Elmer), built around a Nikon Ti-E inverted microscope and controlled by Volocity software (Improvision), was used. Imaging was carried out at 37ºC with a 63x PlanApo oil objective (1.45 NA). A built-in photo-perturbation unit was used to deliver 488nm light pulses in a 5μm^2 area.

Image analysis

Fluorescence images were processed using FIJI (ImageJ; NIH) software. Gaussian blur filters were applied on some of the images presented. For the quantification of the optogenetic experiment, kymographs were built tracing a line across the mitochondria in the unprocessed images, resulting in images like the examples shown in Fig 1G, from which the intensity profile was measured. The fluorescence intensities were normalized to the min and max values using the following formula: $Normalized\ f[t] = \frac{f[t]-f_{min}[t]}{f_{max}[t]-f_{min}[t]}$, where $f[t] = Fmito[t] - Fbkgd[t]$.

Supplemental Material and Methods

For Ca2+ imaging experiments, COS7 cells were seeded and transfected as explained. 2μM thapsigargin (Life Technologies) was added to the medium and Ca2+ was monitored by the intensity of the sensor R-GECO (plasmid was a gift from R. Campbell, Addgene #45494).

VPS13D constructs including the β-propeller region were generated by PCR amplification of the sequences encoding the different portions indicated in Fig S2B and ligation into a pmCherry-C1 backbone by Infusion cloning, using EcoRI and KpnI sites. N-terminal constructs of VPS13D containing the FFAT mutations were generated using site-directed mutagenesis (QuikChange II XL; Agilent technologies).

Supplemental Figure Legends

Figure S1. Miro recruits VPS13D, and not VPS13A, to mitochondria in a Ca^{2+}-independent way. (A) The graph shows relative levels of cytosolic Ca^{2+} concentration in COS7 cells, as monitored by the R-GECO sensor, over time upon application of the SERCA pump inhibitor thapsigargin. Snapshot from selected timepoints, indicated by numbers on the graph, are shown in B. (B) Time-lapse confocal images showing that EGFP-Miro1 recruits VPS13D^Halo to mitochondria independently from cytosolic Ca^{2+} concentration. Scale bar=10μm. (C) Confocal images of VPS13A^Halo co-expressed in COS7 cells along either a mitochondrial marker (mitoGFP) or EGFP-Miro1. Note no obvious differences in the extent of VPS13A recruitment to mitochondria induced by Miro1 transfection. Scale bar=5μm.

Figure S2. The β-propeller region of VPS13D is not sufficient to recruit VPS13D to mitochondria. (A) Cartoon representing full length VPS13D and the VPS13D fragments used in the imaging experiments shown in B. (B) Confocal images of two representative examples of COS7 cells co-expressing mCherry-Miro1 and EGFP-tagged VPS13D fragments showing no mitochondrial recruitment. The VPS13D fragment has a diffuse cytosolic localization with the additional presence of small aggregates in a subset of cells. Scale bar=10μm. (C) List of VPS13D fragments containing the β-propeller region that were tested for Miro-induced recruitment to mitochondria. All of them remained diffuse in the cytosol and/or formed small aggregates, even upon co-expression with Miro1. The constructs used for field B are highlighted in green.

Figure S3. A construct comprising the first 1576 residues of VPS13D is recruited in a VAP-dependent way to the ER. (A) Cartoon representing full length VPS13D and the constructs used for panel C, displaying the localization of the 3 predicted FFAT motifs and the mutations introduced to disrupt them. (B) Sequence and score of each of the 3 predicted FFAT motifs contained in the first 1576 residues of VPS13D. *Score was calculated using a previously described algorithm; scores 3.5 and 4 are considered weak FFAT motifs (Slee and Levine, 2019). (C) Co-expression of an EGFP-tagged N-terminal fragment of VPS13D truncated at residue 1576 with the ER marker mRFP-Sec61β shows no ER recruitment (first column from the left). The same construct is instead robustly recruited to the ER by co-expression with mCherry-VAPB (second column), but not by co-expression of a mutant VAPB which is unable to bind FFAT motifs (third

column). However, the combined disruption of the 3 best predicted FFAT motifs with the point mutations indicated in panel A did not prevent ER recruitment of this VPS13D fragment by VAPB (right column). Scale bar=10µm.

Movie legends

Movie S1: Confocal time-lapse imaging of a COS7 cell co-expressing VPS13D^Halo, mCh-Miro1(ΔTM)-SspB and EGFP-iLID-Mito (not shown) showing recruitment of VPS13D and Miro1 upon blue light irradiation (at 0s) of the area indicated by the white box. VPS13D^Halo stays enriched in mitochondria for a few frames longer than mCh-Miro1(ΔTM)-SspB does. Scale bars=10µm.

Movie S2: Confocal time-lapse imaging of a COS7 cell co-expressing VPS13D^Halo, EGFP-Miro1 and BFP-VAPB upon hypotonic shock. Mitochondria and ER vesiculate but remain tethered by hot spots of VPS13D. Cells were imaged right after water addition at a rate of 0.5 fps for a total of 2 minutes. Some frames were lost due to focal plane changes. Scale bar=3µm.

References

Anding, A.L., C. Wang, T.-K. Chang, D.A. Sliter, C.M. Powers, K. Hofmann, R.J. Youle, and E.H. Baehrecke. 2018. Vps13D Encodes a Ubiquitin-Binding Protein that Is Required for the Regulation of Mitochondrial Size and Clearance. *Curr. Biol.* 28:287–295.e6. doi:10.1016/j.cub.2017.11.064.

Antonicka, H., Z.-Y. Lin, A. Janer, W. Weraarpachai, A.-C. Gingras, and E.A. Shoubridge. 2020. A high-density human mitochondrial proximity interaction network. *BioRxiv*. 2020.04.01.020479.

Berenguer-Escuder, C., D. Grossmann, F. Massart, P. Antony, L.F. Burbulla, E. Glaab, S. Imhoff, J. Trinh, P. Seibler, A. Grünewald, and R. Krüger. 2019. Variants in Miro1 Cause Alterations of ER-Mitochondria Contact Sites in Fibroblasts from Parkinson's Disease Patients. *J Clin Med*. 8:2226. doi:10.3390/jcm8122226.

Dong, R., Y. Saheki, S. Swarup, L. Lucast, J.W. Harper, and Pietro De Camilli. 2016. Endosome-ER Contacts Control Actin Nucleation and Retromer Function through VAP-Dependent Regulation of PI4P. *Cell*. 166:408–423. doi:10.1016/j.cell.2016.06.037.

Dziurdzik, S.K., B.D.M. Bean, M. Davey, and E. Conibear. 2020. A VPS13D spastic ataxia mutation disrupts the conserved adaptor binding site in yeast Vps13. *Hum. Mol. Genet.* 10:1287. doi:10.1093/hmg/ddz318.

Fransson, A., A. Ruusala, and P. Aspenström. 2003. Atypical Rho GTPases have roles in mitochondrial homeostasis and apoptosis. *Journal of Biological Chemistry*. 278:6495–6502. doi:10.1074/jbc.M208609200.

Frederick, R.L., J.M. McCaffery, K.W. Cunningham, K. Okamoto, and J.M. Shaw. 2004. Yeast Miro GTPase, Gem1p, regulates mitochondrial morphology via a novel pathway. *J Cell Biol*. 167:87–98. doi:10.1083/jcb.200405100.

Gauthier, J., I.A. Meijer, D. Lessel, N.E. Mencacci, D. Krainc, M. Hempel, K. Tsiakas, H. Prokisch, E. Rossignol, M.H. Helm, L.H. Rodan, J. Karamchandani, M. Carecchio, S.J. Lubbe, A. Telegrafi, L.B. Henderson, K. Lorenzo, S.E. Wallace, I.A. Glass, F.F. Hamdan, J.L. Michaud, G.A. Rouleau, and P.M. Campeau. 2018. Recessive mutations in VPS13D cause childhood onset movement disorders. *Ann. Neurol.* 83:1089–1095. doi:10.1002/ana.25204.

Glater, E.E., L.J. Megeath, R.S. Stowers, and T.L. Schwarz. 2006. Axonal transport of mitochondria requires milton to recruit kinesin heavy chain and is light chain independent. *J Cell Biol*. 173:545–557. doi:10.1083/jcb.200601067.

Guntas, G., R.A. Hallett, S.P. Zimmerman, T. Williams, H. Yumerefendi, J.E. Bear, and B. Kuhlman. 2015. Engineering an improved light-induced dimer (iLID) for controlling the localization and activity of signaling proteins. *Proc. Natl. Acad. Sci. U.S.A.* 112:112–117. doi:10.1073/pnas.1417910112.

Hung, V., S.S. Lam, N.D. Udeshi, T. Svinkina, G. Guzman, V.K. Mootha, S.A. Carr, and A.Y. Ting. 2017. Proteomic mapping of cytosol-facing outer mitochondrial and ER membranes in living human cells by proximity biotinylation. *eLife*. 6:1206.

doi:10.7554/eLife.24463.

Insolera, R., P. Lorincz, A.J. Wishnie, G. Juhász, and C.A. Collins. 2020. Mitochondrial fission, integrity and clearance require separable functions of Vps13D in Drosophila neurons. 75:1151–41. doi:10.1101/2020.01.21.914523.

John Peter, A.T., B. Herrmann, D. Antunes, D. Rapaport, K.S. Dimmer, and B. Kornmann. 2017. Vps13-Mcp1 interact at vacuole-mitochondria interfaces and bypass ER-mitochondria contact sites. *J Cell Biol*. 216:3219–3229. doi:10.1083/jcb.201610055.

Kanfer, G., T. Courthéoux, M. Peterka, S. Meier, M. Soste, A. Melnik, K. Reis, P. Aspenström, M. Peter, P. Picotti, and B. Kornmann. 2015. Mitotic redistribution of the mitochondrial network by Miro and Cenp-F. *Nature Communications*. 6:8015–9. doi:10.1038/ncomms9015.

King, C., P. Sengupta, A.Y. Seo, and J. Lippincott-Schwartz. 2020. ER membranes exhibit phase behavior at sites of organelle contact. *Proc. Natl. Acad. Sci. U.S.A.* 117:7225–7235. doi:10.1073/pnas.1910854117.

Kolehmainen, J., G.C.M. Black, A. Saarinen, K. Chandler, J. Clayton-Smith, A.-L. Träskelin, R. Perveen, S. Kivitie-Kallio, R. Norio, M. Warburg, J.-P. Fryns, A. de la Chapelle, and A.-E. Lehesjoki. 2003. Cohen syndrome is caused by mutations in a novel gene, COH1, encoding a transmembrane protein with a presumed role in vesicle-mediated sorting and intracellular protein transport. *Am. J. Hum. Genet.* 72:1359–1369. doi:10.1086/375454.

Kornmann, B., C. Osman, and P. Walter. 2011. The conserved GTPase Gem1 regulates endoplasmic reticulum-mitochondria connections. *Proc. Natl. Acad. Sci. U.S.A.* 108:14151–14156. doi:10.1073/pnas.1111314108.

Kornmann, B., E. Currie, S.R. Collins, M. Schuldiner, J. Nunnari, J.S. Weissman, and P. Walter. 2009. An ER-mitochondria tethering complex revealed by a synthetic biology screen. *Science*. 325:477–481. doi:10.1126/science.1175088.

Kumar, N., M. Leonzino, W. Hancock-Cerutti, F.A. Horenkamp, P. Li, J.A. Lees, H. Wheeler, K.M. Reinisch, and P. De Camilli. 2018. VPS13A and VPS13C are lipid transport proteins differentially localized at ER contact sites. *J Cell Biol*. 217:3625–3639. doi:10.1083/jcb.201807019.

Lang, A.B., A.T. John Peter, P. Walter, and B. Kornmann. 2015. ER-mitochondrial junctions can be bypassed by dominant mutations in the endosomal protein Vps13. *J. Cell Biol.* 210:883–890. doi:10.1083/jcb.201502105.

Lees, J.A., and K.M. Reinisch. 2020. Inter-organelle lipid transfer: a channel model for Vps13 and chorein-N motif proteins. *Curr. Opin. Cell Biol.* 65:66–71. doi:10.1016/j.ceb.2020.02.008.

Lesage, S., V. Drouet, E. Majounie, V. Deramecourt, M. Jacoupy, A. Nicolas, F. Cormier-Dequaire, S.M. Hassoun, C. Pujol, S. Ciura, Z. Erpapazoglou, T. Usenko, C.-A. Maurage, M. Sahbatou, S. Liebau, J. Ding, B. Bilgic, M. Emre, N. Erginel-Unaltuna, G. Guven, F. Tison, C. Tranchant, M. Vidailhet, J.-C. Corvol, P. Krack, A.-L. Leutenegger, M.A. Nalls, D.G. Hernandez, P. Heutink, J.R. Gibbs, J. Hardy, N.W. Wood, T. Gasser, A. Durr, J.-F. Deleuze, M. Tazir, A. Destée, E. Lohmann, E. Kabashi, A. Singleton, O. Corti, A. Brice, French Parkinson's Disease Genetics Study (PDG), International Parkinson's Disease Genomics Consortium (IPDGC). 2016. Loss of VPS13C Function in Autosomal-Recessive Parkinsonism Causes Mitochondrial Dysfunction and Increases PINK1/Parkin-Dependent Mitophagy. *Am. J. Hum. Genet.* 98:500–513. doi:10.1016/j.ajhg.2016.01.014.

Li, P., J.A. Lees, C.P. Lusk, and K.M. Reinisch. 2020. Cryo-EM reconstruction of a VPS13 fragment reveals a long groove to channel lipids between membranes. *J Cell Biol*. 219:3593. doi:10.1083/jcb.202001161.

Liu, X., K. Salokas, F. Tamene, Y. Jiu, R.G. Weldatsadik, T. Öhman, and M. Varjosalo. 2018. An AP-MS- and BioID-compatible MAC-tag enables comprehensive mapping of protein interactions and subcellular localizations. *Nature Communications*. 9:1188. doi:10.1038/s41467-018-03523-2.

López-Doménech, G., C. Covill-Cooke, D. Ivankovic, E.F. Halff, D.F. Sheehan, R. Norkett, N. Birsa, and J.T. Kittler. 2018. Miro proteins coordinate microtubule- and actin-dependent mitochondrial transport and distribution. *The EMBO Journal*. 37:321–336. doi:10.15252/embj.201696380.

Macaskill, A.F., J.E. Rinholm, A.E. Twelvetrees, I.L. Arancibia-Carcamo, J. Muir, A. Fransson, P. Aspenström, D. Attwell, and J.T. Kittler. 2009. Miro1 is a calcium sensor for glutamate receptor-dependent localization of mitochondria at synapses. *Neuron*.

61:541–555. doi:10.1016/j.neuron.2009.01.030.

Maeda, S., C. Otomo, and T. Otomo. 2019. The autophagic membrane tether ATG2A transfers lipids between membranes. *eLife*. 8:E3179. doi:10.7554/eLife.45777.

Modi, S., G. López-Doménech, E.F. Halff, C. Covill-Cooke, D. Ivankovic, D. Melandri, I.L. Arancibia-Carcamo, J.J. Burden, A.R. Lowe, and J.T. Kittler. 2019. Miro clusters regulate ER-mitochondria contact sites and link cristae organization to the mitochondrial transport machinery. *Nature Communications*. 10:4399–15. doi:10.1038/s41467-019-12382-4.

Murphy, S.E., and T.P. Levine. 2016. VAP, a Versatile Access Point for the Endoplasmic Reticulum: Review and analysis of FFAT-like motifs in the VAPome. *Biochim. Biophys. Acta*. 1861:952–961. doi:10.1016/j.bbalip.2016.02.009.

Nguyen, T.T., S.S. Oh, D. Weaver, A. Lewandowska, D. Maxfield, M.-H. Schuler, N.K. Smith, J. Macfarlane, G. Saunders, C.A. Palmer, V. Debattisti, T. Koshiba, S. Pulst, E.L. Feldman, G. Hajnóczky, and J.M. Shaw. 2014. Loss of Miro1-directed mitochondrial movement results in a novel murine model for neuron disease. *Proc. Natl. Acad. Sci. U.S.A.* 111:E3631–40. doi:10.1073/pnas.1402449111.

Oeding, S.J., K. Majstrowicz, X.-P. Hu, V. Schwarz, A. Freitag, U. Honnert, P. Nikolaus, and M. Bähler. 2018. Identification of Miro1 and Miro2 as mitochondrial receptors for myosin XIX. *J Cell Sci*. 131:jcs219469. doi:10.1242/jcs.219469.

Okumoto, K., T. Ono, R. Toyama, A. Shimomura, A. Nagata, and Y. Fujiki. 2018. New splicing variants of mitochondrial Rho GTPase-1 (Miro1) transport peroxisomes. *J Cell Biol*. 217:619–633. doi:10.1083/jcb.201708122.

Osawa, T., T. Kotani, T. Kawaoka, E. Hirata, K. Suzuki, H. Nakatogawa, Y. Ohsumi, and N.N. Noda. 2019. Atg2 mediates direct lipid transfer between membranes for autophagosome formation. *Nat. Struct. Mol. Biol.* 26:281–288. doi:10.1038/s41594-019-0203-4.

Park, J.-S., M.K. Thorsness, R. Policastro, L.L. McGoldrick, N.M. Hollingsworth, P.E. Thorsness, and A.M. Neiman. 2016. Yeast Vps13 promotes mitochondrial function and is localized at membrane contact sites. *Molecular Biology of the Cell*. 27:2435–2449. doi:10.1091/mbc.E16-02-0112.

Rampoldi, L., C. Dobson-Stone, J.P. Rubio, A. Danek, R.M. Chalmers, N.W. Wood, C. Verellen, X. Ferrer, A. Malandrini, G.M. Fabrizi, R. Brown, J. Vance, M. Pericak-Vance, G. Rudolf, S. Carrè, E. Alonso, M. Manfredi, A.H. Németh, and A.P. Monaco. 2001. A conserved sorting-associated protein is mutant in chorea-acanthocytosis. *Nat. Genet.* 28:119–120. doi:10.1038/88821.

Saotome, M., D. Safiulina, G. Szabadkai, S. Das, A. Fransson, P. Aspenström, R. Rizzuto, and G. Hajnóczky. 2008. Bidirectional Ca2+-dependent control of mitochondrial dynamics by the Miro GTPase. *Proc. Natl. Acad. Sci. U.S.A.* 105:20728–20733. doi:10.1073/pnas.0808953105.

Schormair, B., D. Kemlink, B. Mollenhauer, O. Fiala, G. Machetanz, J. Roth, R. Berutti, T.M. Strom, B. Haslinger, C. Trenkwalder, D. Zahorakova, P. Martasek, E. Ruzicka, and J. Winkelmann. 2018. Diagnostic exome sequencing in early-onset Parkinson“s disease confirms VPS13C as a rare cause of autosomal-recessive Parkinson”s disease. *Clin. Genet.* 93:603–612. doi:10.1111/cge.13124.

Seifert, W., J. Kühnisch, T. Maritzen, D. Horn, V. Haucke, and H.C. Hennies. 2011. Cohen syndrome-associated protein, COH1, is a novel, giant Golgi matrix protein required for Golgi integrity. *J. Biol. Chem.* 286:37665–37675. doi:10.1074/jbc.M111.267971.

Seong, E., R. Insolera, M. Dulovic, E.-J. Kamsteeg, J. Trinh, N. Brüggemann, E. Sandford, S. Li, A.B. Ozel, J.Z. Li, T. Jewett, A.J.A. Kievit, A. Münchau, V. Shakkottai, C. Klein, C.A. Collins, K. Lohmann, B.P. van de Warrenburg, and M. Burmeister. 2018. Mutations in VPS13D lead to a new recessive ataxia with spasticity and mitochondrial defects. *Ann. Neurol.* 83:1075–1088. doi:10.1002/ana.25220.

Shlevkov, E., T. Kramer, J. Schapansky, M.J. LaVoie, and T.L. Schwarz. 2016. Miro phosphorylation sites regulate Parkin recruitment and mitochondrial motility. *Proc. Natl. Acad. Sci. U.S.A.* 113:E6097–E6106. doi:10.1073/pnas.1612283113.

Slee, J.A., and T.P. Levine. 2019. Systematic prediction of FFAT motifs across eukaryote proteomes identifies nucleolar and eisosome proteins with the predicted capacity to form bridges to the endoplasmic reticulum. *Contact (Thousand Oaks)*. 2:1–21. doi:10.1177/2515256419883136.

Ueno, S., Y. Maruki, M. Nakamura, Y. Tomemori, K. Kamae, H. Tanabe, Y. Yamashita, S. Matsuda, S. Kaneko, and A. Sano. 2001. The gene encoding a newly discovered protein, chorein, is mutated in chorea-acanthocytosis. *Nat. Genet.* 28:121–122. doi:10.1038/88825.

Ugur, B., W. Hancock-Cerutti, M. Leonzino, and P. De Camilli. 2020. Role of VPS13, a protein with similarity to ATG2, in physiology and disease. *Current Opinion in Genetics & Development*. 65:61–68. doi:10.1016/j.gde.2020.05.027.

Valverde, D.P., S. Yu, V. Boggavarapu, N. Kumar, J.A. Lees, T. Walz, K.M. Reinisch, and T.J. Melia. 2019. ATG2 transports lipids to promote autophagosome biogenesis. *J Cell Biol*. 14:jcb.201811139. doi:10.1083/jcb.201811139.

Velayos-Baeza, A., A. Vettori, R.R. Copley, C. Dobson-Stone, and A.P. Monaco. 2004. Analysis of the human VPS13 gene family. *Genomics*. 84:536–549. doi:10.1016/j.ygeno.2004.04.012.

Wang, X., and T.L. Schwarz. 2009. The mechanism of Ca2+ -dependent regulation of kinesin-mediated mitochondrial motility. *Cell*. 136:163–174. doi:10.1016/j.cell.2008.11.046.

Wang, X., D. Winter, G. Ashrafi, J. Schlehe, Y.L. Wong, D. Selkoe, S. Rice, J. Steen, M.J. LaVoie, and T.L. Schwarz. 2011. PINK1 and Parkin target Miro for phosphorylation and degradation to arrest mitochondrial motility. *Cell*. 147:893–906. doi:10.1016/j.cell.2011.10.018.

Yeshaw, W.M., M. van der Zwaag, F. Pinto, L.L. Lahaye, A.I. Faber, R. Gómez-Sánchez, A.M. Dolga, C. Poland, A.P. Monaco, S.C. van IJzendoorn, N.A. Grzeschik, A. Velayos-Baeza, and O.C. Sibon. 2019. Human VPS13A is associated with multiple organelles and influences mitochondrial morphology and lipid droplet motility. *eLife*. 8:728. doi:10.7554/eLife.43561.

Figure1: (2 columns)

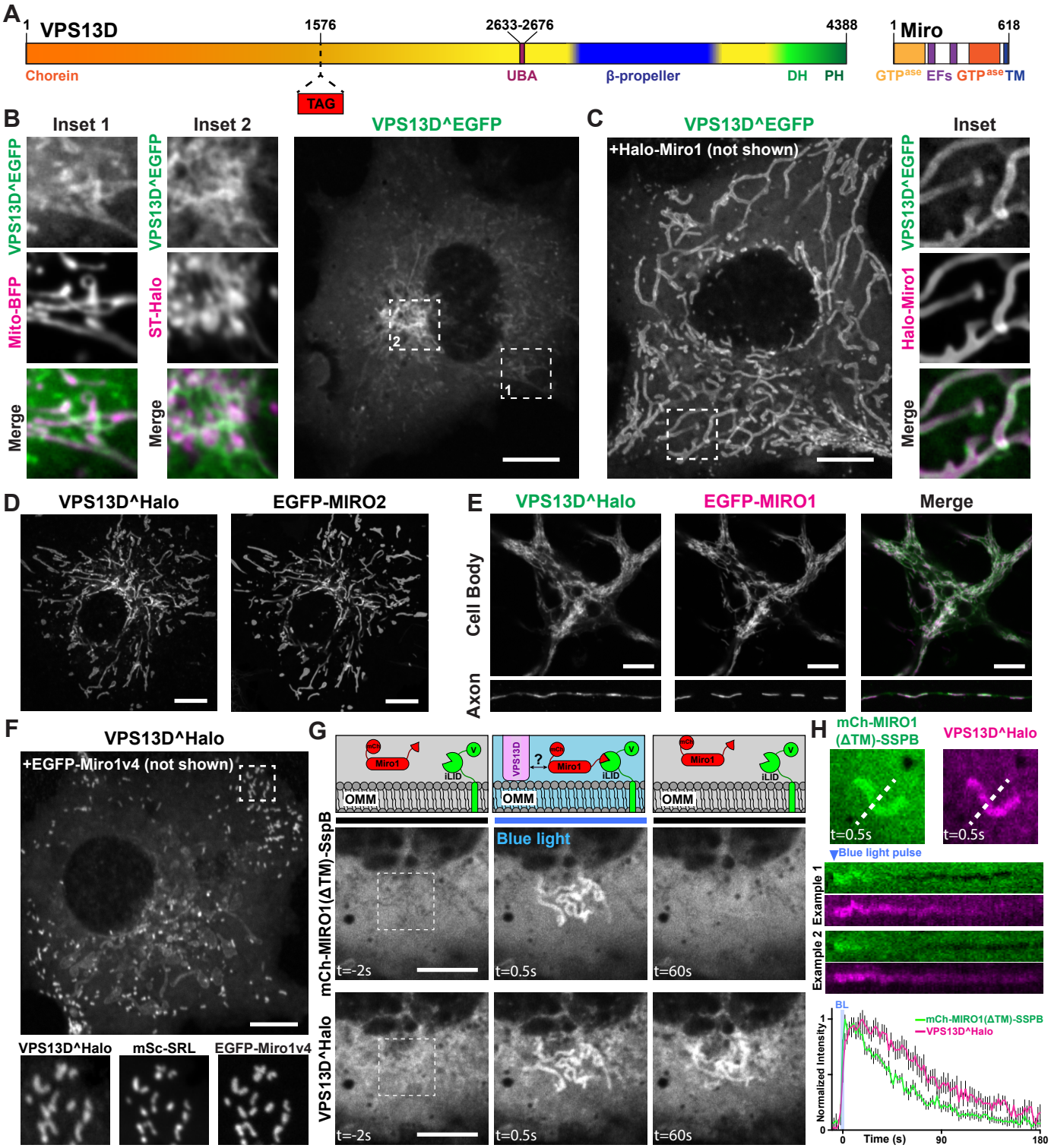

Figure2: 1 column figure

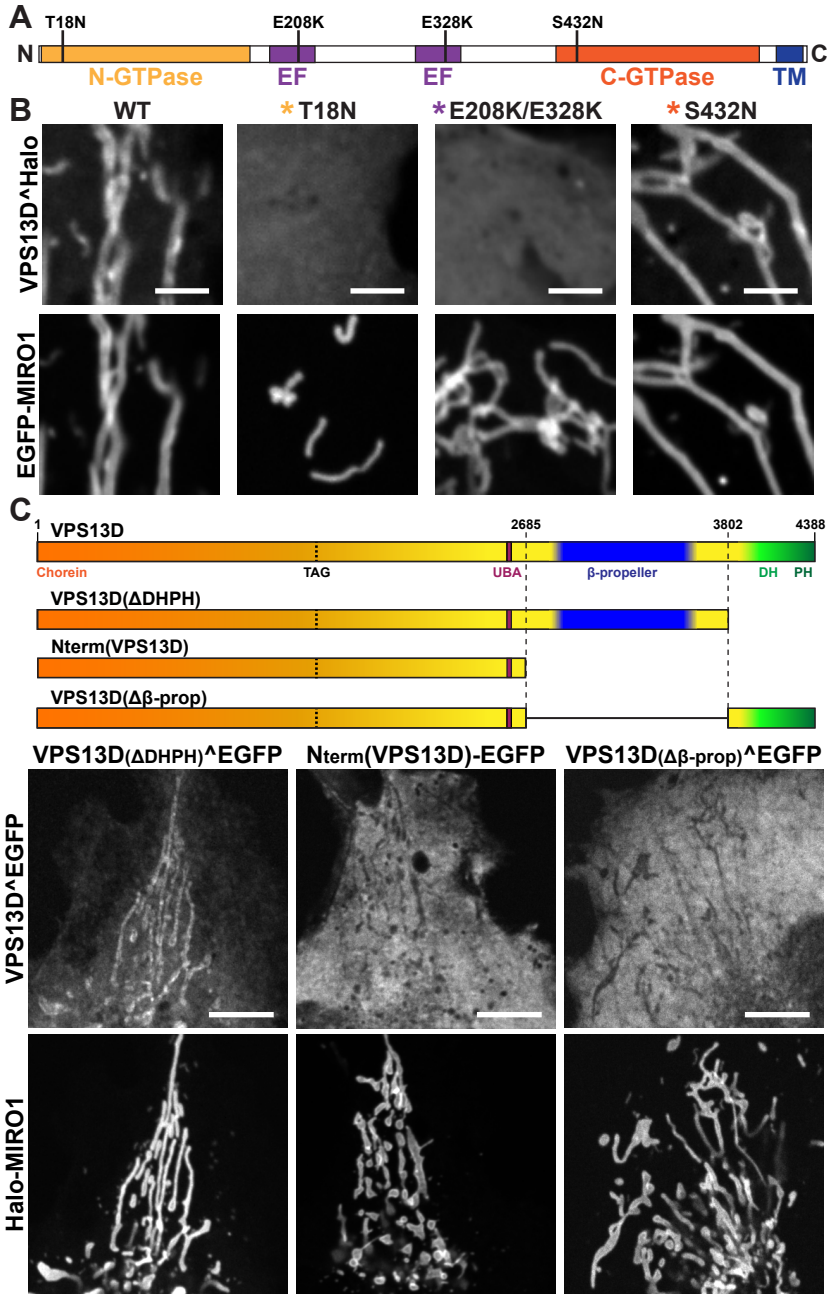

Figure 3: (2 columns)

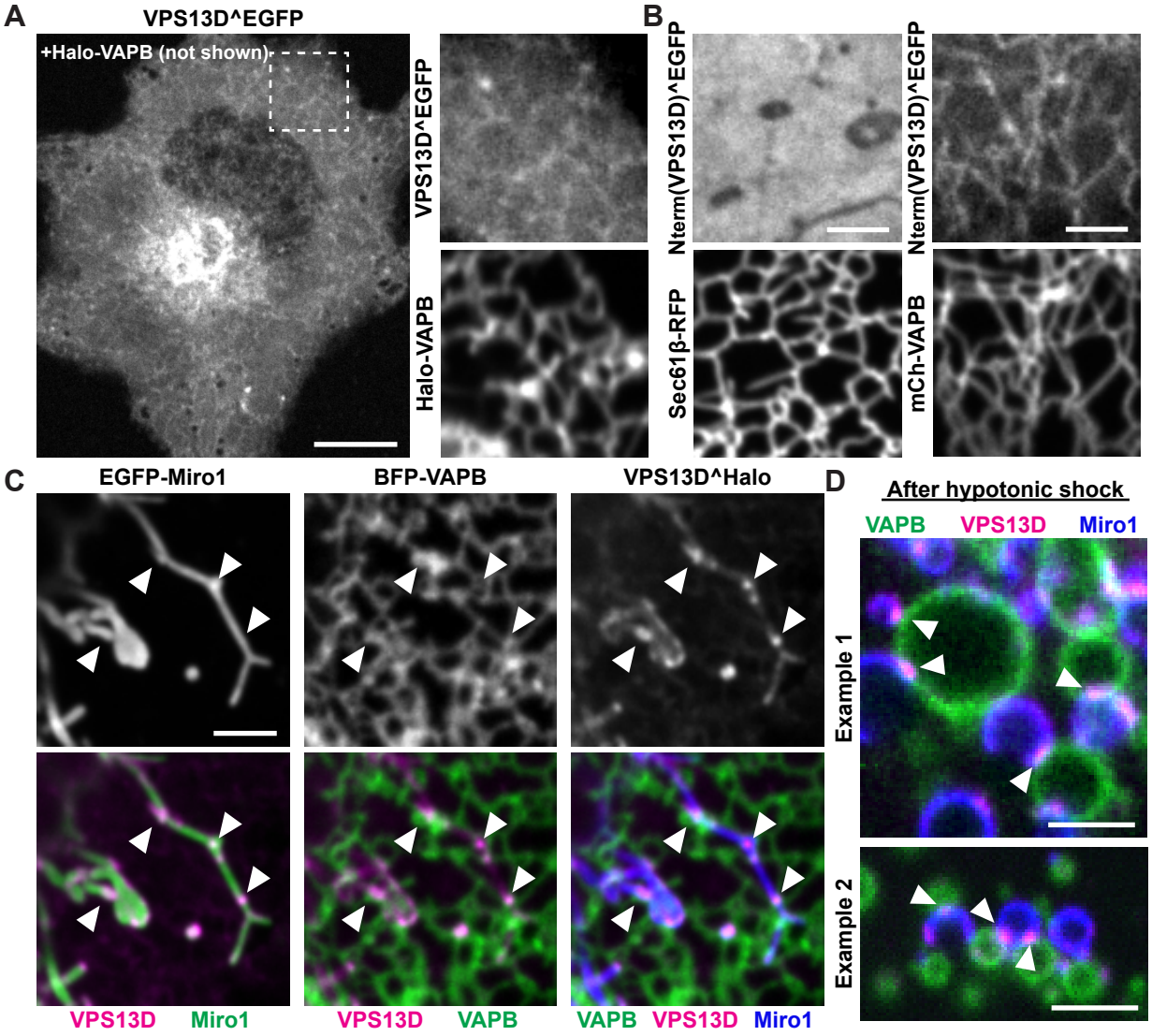

Figure S1

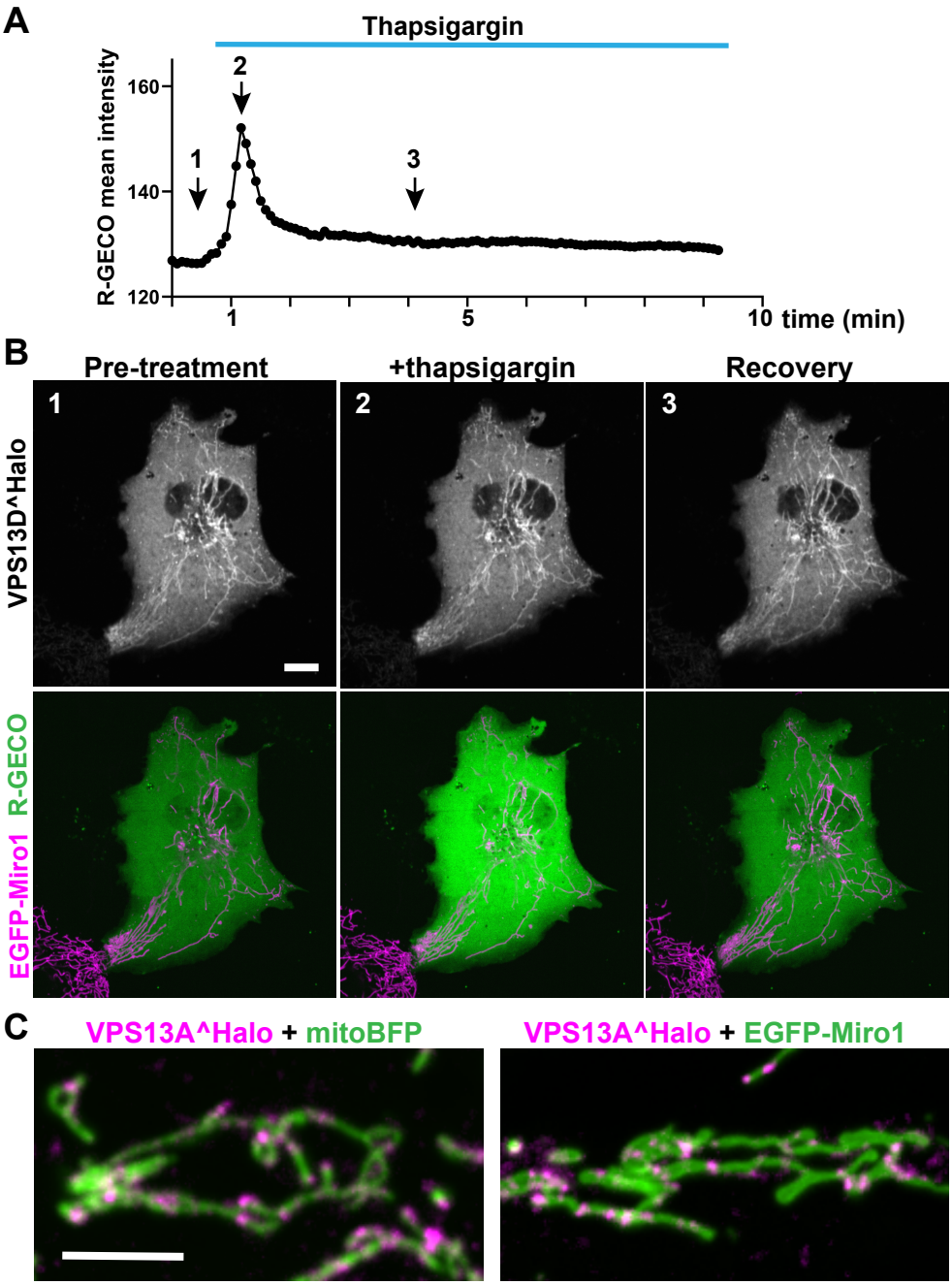
A
Thapsigargin
R-GECO mean intensity
160
140
120
1
2
3
1
5
10
time (min)
B
Pre-treatment
+thapsigargin
Recovery
VPS13D^Halo
EGFP-Miro1
R-GECO
C
VPS13A^Halo + mitoBFP
VPS13A^Halo + EGFP-Miro1

Figure S2

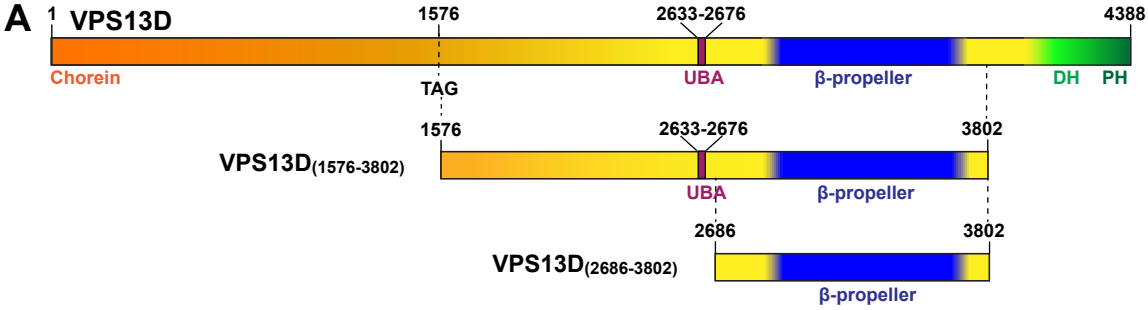

B

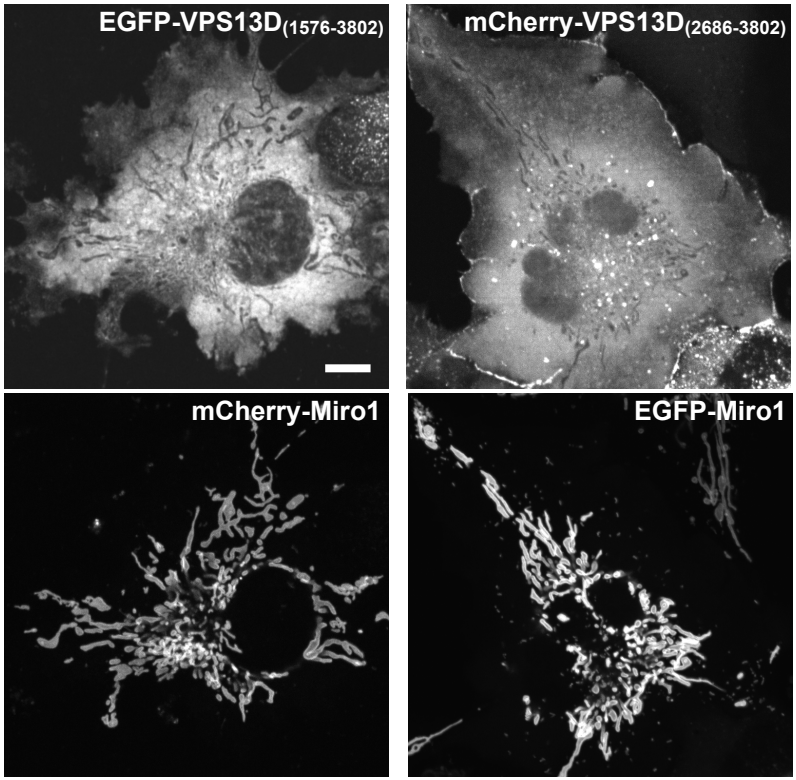

C

aa start	aa end	Localization
2880	3945	Cyt
2875	3812	Cyt
1576	3802	Cyt
2079	3802	Cyt
2176	3802	Cyt
2434	3802	Cyt
2686	3802	Cyt
2887	3802	Cyt
2887	3557	Cyt
2887	3610	Cyt
2887	3675	Cyt
2887	3750	Cyt
2881	3579	Cyt

Figure S3

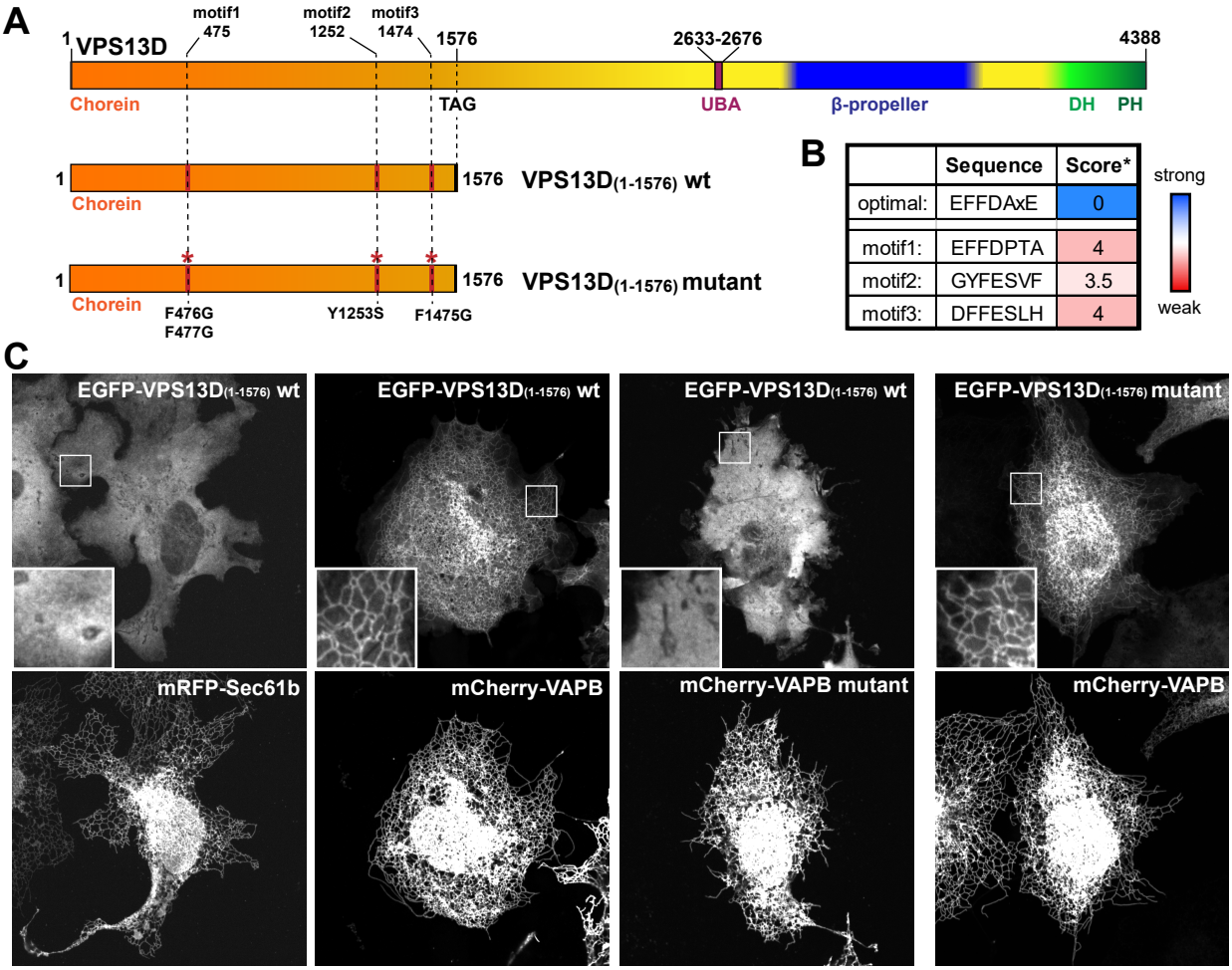

	Sequence	Score*
optimal:	EFFDAxE	0
motif1:	EFFDPTA	4
motif2:	GYFESVF	3.5
motif3:	DFFESLH	4

Table S1: List of primers used in this study

Construct	Cloning method	Template	Primer sequence	Backbone
VPS13D Fragments				
mCherry-VPS13D (1576-3802)	Infusion	**Backbone: pmCherry-C1**	CGGATCTAGATAACTGATCATAATC	pmCherry-C1
			TGCAGAATTCGAAGCTTGAG	
		VPS13D	CGCTAGCGCTACCGGGCCACCATGGTGAGCAAGG	
			GTCGACTGCAGAATTGGACCGGGAGCTCTTGCG	
VPS13D(1-1576)-EGFP	HIFi	**VPS13D**	tttagtgaaccgtcagatcc*gccacc*ATGCTGGAGGGCCTGGTC	pEGFP-N1
			accatggtggcgaccggtggAGAGGAGCCAGAGCCTGG	
		Backbone: pEGFP-N1	CCACCGGTCGCCACCATG	
			GGATCTGACGGTTCACTAAACCAGC	
VPS13D^Halo	Infusion	**pHalo-C1**	TGGCTCCTCTGGATCCGCCACCATGGCAGAAATCGG	VPS13D^mSc (BamHI)
			GGGGTCCTCCGGATCCTCCGGACTTGTACAGGCCG	
VPS13D^EGFP	Infusion	**pEGFP-C1**	TGGCTCCTCTGGATCCGCCACCATGGTGAGCAAGG	VPS13D^mSc (BamHI)
			GGGGTCCTCCGGATCCAGATCTGAGTCCGGACTTGTACAGC	
Nterm(VPS13D)^EGFP	Infusion	**VPS13D^EGFP**	AGATCCGCTAGCGCTACCGGccaccATGCTGGAGGGCCTGGTC	pEGFP_C1 (AgeI, EcoRI)
			GTCGACTGCAGAATTaTCCAGGGCTGTCCCTGCTG	
VPS13D(Δβ-prop)^EGFP	Infusion	**VPS13D^EGFP (1st insert)**	AGATCCGCTAGCGCTACCGGccaccATGCTGGAGGGCCTGGTC	pEGFP_C1 (AgeI, EcoRI)
			ACCGGGAGCTTCCAGGGCTGTCCCTGCTG	
		VPS13D^EGFP (2nd insert)	CAGCCCTGGAAGCTCCCGGTCCTATGAGG	
			GTACCGTCGACTGCAGAATTTTATGAATCCAGTTCCAGCTGTT	
VPS13D(ΔDHPH)^EGFP	Quikchange Mutagenesis	**VPS13D^EGFP**	CTCATCCACCTCATTAGGACCGGGAGCTCTT	VPS13D^EGFP
			AAGAGCTCCCGGTCCTAATGAGGTGGATGAG	
EGFP-Miro1	Infusion	**myc-Miro1**	GGACTCAGATCTCGAGtgGGATCTATGAAGAAAGACGTGCGG	pEGFP_C1 (EcoRI, XhoI)
			GTCGACTGCAGAATTCTCATCGCTGTTTCAATAATGCTTTG	
EGFP-Miro2	Infusion	**myc-Miro2**	GGACTCAGATCTCGAGTGGGATCTATGAGGCGGGAC	pEGFP_C1 (EcoRI, XhoI)
			GTCGACTGCAGAATTCTCACTGGCTCTTCACCAGGAC	
EGFP-Miro1v4	Infusion	**EGFP-Miro1**	CACGTGACACAAGCTGACC	
			GGATACATGGCCATTGTTGTC	
		v4 amplification	AATGGCCATGTATCCAGAGGATCATTACAGAGACAGACTC	

			AGCTTGTGTCACGTGCCTGTTAAGAACTGCAGTGAAG	EGFP-Miro1 (linearized by PCR)
		gBlock containing v4 seq	ATAGACGGCAACTAAGAGGATCATTACAGAGACAGACTCTCC CGAGACATGGGCCACACTGATAGAATAGAGAATTTGAGAAAA ATCTGGGTCTTTCTAAAAACTGCTTTCCATGCCCGGTTACGC TGTATGTGCACCTGCAACAGGTGTACATTTTGCATCTGTCAG AACTTCCTCAACTCAGACTTGCTGCAATCTGTAAAGAACAAA ATCTTCACTGCAGTTCTTAACAGGGACGGCAACTAAGT	
mCh-Miro1(ΔTM)-SspB	Infusion	**EGFP-Miro1**	TCGAGCTCAAGCTTCGAATTTGGGATCTATGAAGAAAGACGTG	pmCherry-C1 (EcoRI, KpnI)
			GAGCTCGAGAGCTCTTGAGGTCAGCTTGTGTC	
		tgRFPt-SspB	CCTCAAGAGCTCTCGAGCTCAAGCTTCG	
			CGGTGGATCCCGGGCCCGCGTTAACCAATATTCAGCTCGTCAT	
VPS13D and Miro mutants				
VPS13D(1-1576)-Y1253S	Quikchange	**VPS13D (1-1576)**	CATCTCTGATATCGGCTcTTTCGAGAGCGTGTTTGTGC	pEGFP-N1
			GCACAAACACGCTCTCGAAAgAGCCGATATCAGAGATG	
EGFP-Miro1 (T18N)	Quikchange Mutagenesis	**EGFP-Miro1**	AGACATAATCAGTGAGTTCTTCCCAACTCTAGGTTCTCCCAC	EGFP-Miro1
			GTGGGAGAACCTAGAGTTGGGAAGAACTCACTGATTATGTCT	
EGFP-Miro1 (E208K)	Quikchange Mutagenesis	**EGFP-Miro1**	CCTCTGAAAGAAGTTGAGTTTAGCATCATTGAGAGTACCAT	EGFP-Miro1
			ATGGTACTCTCAATGATGCTAAACTCAACTTCTTTCAGAGG	
EGFP-Miro1 (E328K)	Quikchange Mutagenesis	**EGFP-Miro1**	TTTAAATAAATCTTTAAGCTTATCAGGTGACAAAGCACAGTC TCTATC	EGFP-Miro1
			GATAGAGACTGTGCTTTGTCACCTGATAAGCTTAAAGATTTA TTTAAA	
EGFP-Miro1 (S432N)	Quikchange	**EGFP-Miro1**	GCCTGAAGAACTCCATTTTTCCCACAGTTTTTCACTC	EGFP-Miro1
			GAGTGAAAAACTGTGGGAAAAATGGAGTTCTTCAGGC	
Other Constructs				
BFP-VAPB	HiFi	**tagBFP**	cgctaccggtcgccaccatgAGCGAGCTGATTAAGGAG	pmCherry-C1
			gctcgagatctgagtccggaATTAAGCTTGTGCCCCAG	
		VAPB	TCCGGACTCAGATCTCGAG	
			CATGGTGGCGACCGGTAG	
Halo-VAPB	Infusion	**VAPB**	CTCAAGCTTCGAATTCtATGGCGAAGGTGGAGCAG	pHALO-C1 (EcoRI, KpnI)
			GATCCCGGGCCCGCGGTACCCTACAAGGCAATCTTCCCAATA A	

Sialyltransferase-Halo	Infusion	**Sialyltransferase**	CTCAAGCTTCGAATTccaccATGATTCACACCAACCTGAAG	pHALO-N1 (EcoRI, KpnI)
			GATCCCGGGCCCGCGtGGAATTCCCCTTGGTTTGC	